CCIT Report #618, April 2007

Capabilities and limitations of paraxial operator approach for modeling of nano-scale feature evaluation

Alexander Normatov, Boris Spektor, Joseph Shamir
Electrical Engineering Department, Technion – Israeli Institute of Technology; Technion City, Haifa 32000, Israel;

ABSTRACT

The interaction of light with nano-scale features is usually associated with rigorous vector modeling or other computation intensive method. It turns out, however, that several interesting cases can be analyzed by a model based on scalar, paraxial operators. Good correspondence was found between this theoretical model and experimental investigation. In our work, the capabilities of scalar, paraxial operator approach are discussed for the cases of Dark beam and Gaussian beam scanning microscopes. Fundamental limitations of the approach are outlined as well. The sensitivity of the Dark beam scanning microscope was compared for the real experimental procedure and the idealized theoretical model which indicated a potential of 1nm sensitivity.

Keywords: Dark beam, nano-scale, microscopy, modeling

1. INTRODUCTION

Progress in high-tech production, such as optical components, flat panel displays and semiconductor industry places increasingly stringent requirements on surface quality. As a result, there is a constantly growing demand for high-sensitivity and high-speed inspection systems operating in the production lines. Since traditional methods do not provide an adequate answer to industrial needs, other, more sophisticated methods were developed. Among these methods, Dark Beam (DB) microscopy was proposed[1-3] and preliminary investigations indicated high performance capabilities.

In Ref. 4 we have analyzed a generalized version of DB microscopy, Singular Beam (SB) microscopy, both experimentally and by numerical simulations, demonstrating nanoscale sensitivity. The simulations were carried out with the help of operator representation[5] within the regime of paraxial optics approximation. The purpose of this paper is to discuss those simulations and estimate their validity for analyzing systems designed to investigate nanoscale features.

Choosing a particular method of analysis usually involves a tradeoff between the allowed errors and availability of computational resources and processing time. In this paper we demonstrate that the scalar paraxial approximation produces reasonably accurate results for optical systems with numerical apertures (NA) up to 0.4. The next section provides a general background on the SB microscopy and this is followed in Sect. 3 with a discussion of the DB microscopy as a particular case of the SB microscopy. Section 4 compares scalar, paraxial results with experiments and with rigorous vector calculations to estimate the introduced errors. Section 5 evaluates the implications of inaccuracies on the sensitivity of the microscopy approach. Finally, the conclusions are drawn in section 6.

2. SINGULAR BEAM MICROSCOPY

The main idea of SB microscopy can be outlined as follows. The space, containing the investigated object is scanned by a focused beam containing singularities. Light scattered by the object propagates in free space and/or through optical elements to a recording system where it is analyzed to evaluate required object features. Since SB microscopy does not deal with direct optical imaging, the classical diffraction limit is mitigated and system performance is constrained only by the Signal to Noise Ratio (SNR) of the measured data.

2.1 Singular beams and their generation

Optical singularities and their properties are subject for extensive study.[6-10] A wide variety of optical singularities exists. These can be optical vortices, other kind of phase singularities or polarization singularities.[11-17] Our main interest here is in beams containing one or more phase singularities that generate spatial regions where the complex amplitude vanishes.

Singularities can be introduced in a conventional beam with the help of a diffractive optical element,[18] or can be generated directly within the laser cavity.[19] Although, generally SB microscopy deals with either one dimensional or two dimensional singularities, in this work we restrict ourselves to a specific 1D singularity, a line phase dislocation. This singularity was introduced into a Gaussian beam by means of a π phase step and consequent spatial filtering.

2.2 Singular beam microscope

A possible optical setup for SB microscopy in transmission mode is presented in Fig. 1. A Gaussian laser beam is modulated by a phase mask that introduces one or more optical singularities. The SB is focused by a microscope objective into the sample space where it interacts with the investigated object and the scattered intensity distribution reaches the recording plane.

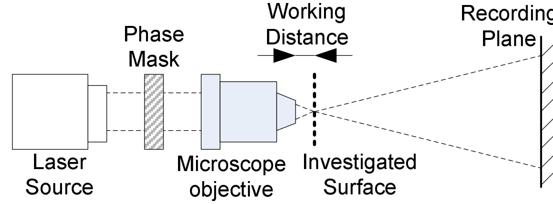

Fig. 1. Schematic diagram of a singular beam microscope. A Gaussian laser beam passes through a phase mask that introduces optical singularities and is focused into the investigated space. Light scattered by the object is measured at the recording plane.

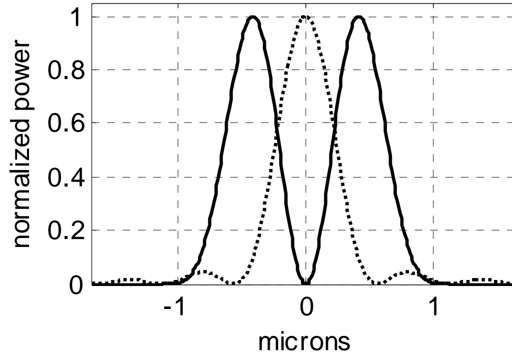

Fig. 2. Cross section of the intensity distribution at the focal plane of the microscope objective with NA = 0.4 for an idealized SB (solid curve) and the corresponding Gaussian intensity distribution (dotted curve). The intensities are normalized to 1.

The simulated cross section of the intensity distribution for an idealized SB is shown in Fig. 2 as compared to a corresponding Gaussian Beam. Both intensity profiles are at the focal plane of a microscope objective with NA = 0.4. The vanishing of the intensity at the center of the SB is a result of the phase dislocation that generates the anti-symmetric complex amplitude distribution as shown in Fig. 3. The two intensity lobes of the SB can be viewed as two arms of an interferometer that can intuitively explain why nanoscale sensitivity is possible.

2.3 Modeling of singular beam microscope

Paraxial, scalar operator representation of the above system (Fig. 1), is given according to the operator definitions[5]. The wavefront entering the microscope objective can be written as,

$$U_{in} = R\left[d_2\right]T_{mask}A\frac{q_0 e^{jkd_1}}{q(d_1)}Q\left[\frac{1}{q(d_1)}\right], \tag{1}$$

where d_1 is the distance between the laser beam waist and the phase mask (represented as a thin optical element with transfer function T_{mask}) and d_2 is the distance between the phase mask and the microscope objective. The Gaussian beam

amplitude is *A* and free space propagation is represented in a short hand notation by the Free Space Propagation operator, *R*, which can be expressed by a cascade of fundamental operators. Two such expressions are,

$$R[d] = e^{jkd} F Q\left[-\lambda^2 d\right] F^{-1}$$
$$R[d] = \frac{e^{jkd}}{j\lambda d} Q\left[\frac{1}{d}\right] V\left[\frac{1}{\lambda d}\right] Q\left[\frac{1}{d}\right] \qquad (2)$$

where *d* is the propagation distance, λ is the free space wavelength and $k = 2\pi/\lambda$ is the wave number. Fourier transformation is represented by *F*, scaling by *V* and the quadratic phase factor in one dimension is defined as,

$$Q\left[\frac{1}{a}\right] = e^{\frac{jk}{2a}x^2}, \qquad (3)$$

where *x* is lateral dimension. Finally, in Eq. (1), $q(d) = q_0 + d$, where the Gaussian beam characteristic value, q_0, is:

$$q_0 = \frac{2j}{kw_0^2} = \frac{j\lambda}{\pi w_0^2} \qquad (4)$$

with w_0 denoting the Gaussian beam waist radius. The wavefront U_{in} is focused by the microscope objective to the focal plane where it illuminates the investigated object. In this work we assume that an investigated object can be represented by a thin optical element with transmittance function, T_{obj}. This function accounts for the object features we intend to evaluate. For a perfect microscope objective of focal length *f*, the wavefront at the recording plane, situated at distance d_3 from the focal plane, can be written as,

$$U_{out} = R[d_3] T_{obj} R[f] T_{aperture} Q\left[\frac{-1}{f}\right] U_{in}. \qquad (5)$$

Here $T_{aperture}$ represents the aperture of the microscope objective (usually $T_{aperture} = circ(x/r_{aperture})$, where $r_{aperture}$ is the aperture radius). The intensity distribution at the recording plane (output intensity distribution) can be written as,

$$I_{out} = \left|U_{out}\right|^2. \qquad (6)$$

Similarly, the intensity distribution at the focal plane (as the one shown in Fig. 2) can be written as,

$$I_{focal} = \left| R[f] T_{aperture} Q\left[\frac{-1}{f}\right] U_{in} \right|^2 \qquad (7)$$

While for a Gaussian beam illumination, $T_{mask} = 1$, a singular beam with phase singularity is generated by

$$T_{mask} = e^{jt(x)}, \qquad (8)$$

where the function $t(x)$ contains the desired singularities.

3. DARK BEAM MICROSCOPY

As it was indicated above, DB microscopy is a special case of SB microscopy, where, according to Eq. (8),

$$t(x) = \pi u(x); \quad u(x) = \begin{cases} 0 & x < 0 \\ 1 & x \geq 0 \end{cases} \qquad (9)$$

The examination of the complex amplitude at the focal plane of the microscope objective, as written in Eq. (10), shows a zero-crossing by the amplitude, thus generating absolute zero intensity in the center of I_{focal}, as shown in Fig. 3.

$$U_{focal} = R\left[f\right]T_{aperture}Q\left[\frac{-1}{f}\right]U_{in} \tag{10}$$

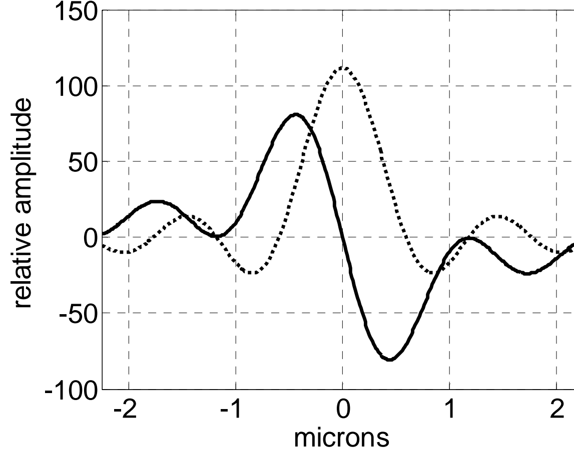

Fig. 3. Dark Beam complex amplitude (solid line) vs. corresponding Gaussian complex amplitude (dotted line) at the microscope objective's focal plane (where the scanned surface is situated).

A comparison between Fig. 2 and Fig. 3 reveals excessive energy outside the two main lobes of the DB. These “tails”, situated outside ±1.2 microns from the center, are the product of convolution of the DB focal wavefront with the Fourier transform of the aperture function. Obviously, these tails are undesirable, as they may interact with the investigated object situated outside the DB main lobes, thus reducing the overall SNR of the system. Effective suppression of these tails can be accomplished with a proper spatial filtering.

3.1 Recorded intensity distribution analysis

In the experimental study of a DB microscope, as special case of a SB microscope[4], a π phase step was used as a test object that can be described by the transmittance function, $T_{obj} = e^{j\pi u(x-x_n)}$. The recorded intensity distribution (output distribution) I_{out}, along with the simulation results are presented in Figs. 4 and 5. The relative position between the phase step and the DB center was controlled by x_n that was gradually changed between consecutive measurements. In view of the nanoscale nature of the experiments the differences among experimental intensity distribution profiles are reasonable.

In a typical experiment the investigated object (π phase step) scans through all the DB focal intensity distribution. In order to facilitate the comparison, an integration window was introduced in the center of the intensity distribution. The place for the integration window was chosen in the center since the changes between the intensity distribution profiles are most pronounced there and the distortions are minimal. The value of the total power in the window can be plotted against the phase step position as shown in Figure 6. Although the experimental curves are slightly wider (due to imperfections), the overall similarity between the obtained experimental data and the simulation results are apparent.

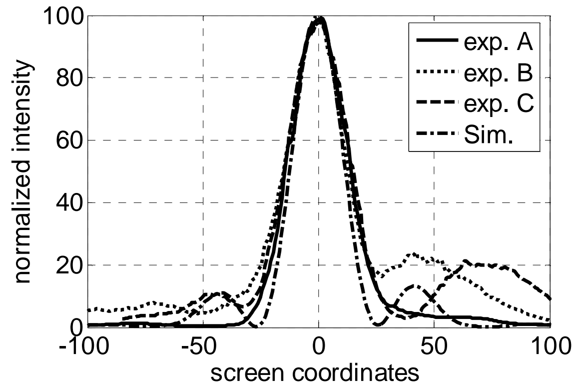

Fig. 4. Recording plane intensity distribution profiles with the phase step positioned at the center of the DB.. Semi dotted curve – simulation, other curves experiments. The Screen coordinates correspond to recording plane coordinates.

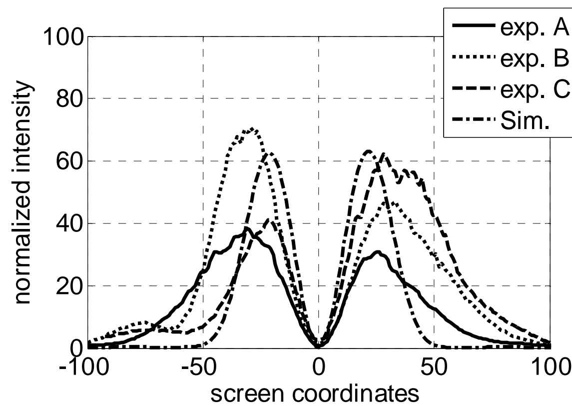

Fig. 5. Same as Fig. 4 but with the phase step positioned outside the DB.

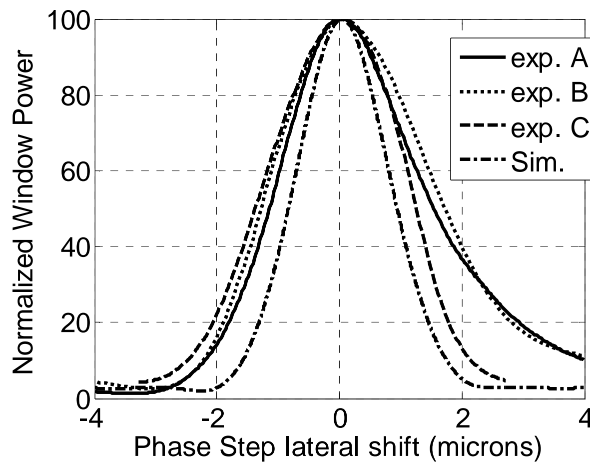

Fig. 6. Integration window power as a function of phase step position. Vertical axis is relative power, horizontal axis is phase step position in microns. Semi dotted curve is simulation, other curves – experiments.

3.2 DB microscopy limitations

Alongside clear advantages of DB microscopy for industrial applications some disadvantages and limitations should be discussed. The main disadvantage is that some *a priori* information about the investigated object is needed before the measured data can be analyzed. This disadvantage is irrelevant for many industrial applications where the object is

known and only its various parameters must be evaluated. The second limitation of DB microscopy is the fact that it extracts information about investigated object features rather than its image. Therefore, DB microscopy is evaluated with a sensitivity metric rather than with a resolution value. Again, industry is usually much more interested in evaluating object features than in visualizing them. Finally, at the current stage DB microscopy is studied only for certain class of isolated objects (like steps, trenches and bars).

4. PARAXIAL APPROXIMATION ERROR ESTIMATION

The choice of paraxial, scalar numerical approximation for nanoscale investigations removes much of the computational complexity, thus enabling real-time, on-line processing. Unfortunately, however, this approximation introduces errors that must be kept in mind when interpreting numerical results. The error estimation will concentrate on two main sources: errors due to violation of the paraxial approximation by large NA systems (NA = 0.4 in our case) and errors due to approximation of nanoscale features by thin optical element.

4.1 Numerical aperture error

In order to assess the influence of the NA(=0.4) on the wave field, a numerical simulation was performed following Ref. 20. The simulation used an incoming plane wave polarized along the x axis and focused by a lens with NA = 0.4. The resulting electric field (taken along x and y at the focal plane to account for ellipticity) is compared with the field value calculated according to Eq. (10), setting U_{in} to be a plane wave. The comparison is made by the rigorously calculated field intensity from its values obtained by the paraxial approximation. This difference is shown in Fig. 7, in percents of the peak intensity calculated by the paraxial approximations. It must be noted that the scalar result was obtained using the Abbe Sine Condition adjustment for the lens aperture. The resulting maximum difference is well below 1%, thus implying that the inaccuracy of the paraxial approximation is below this value for systems with NA≤0.4.

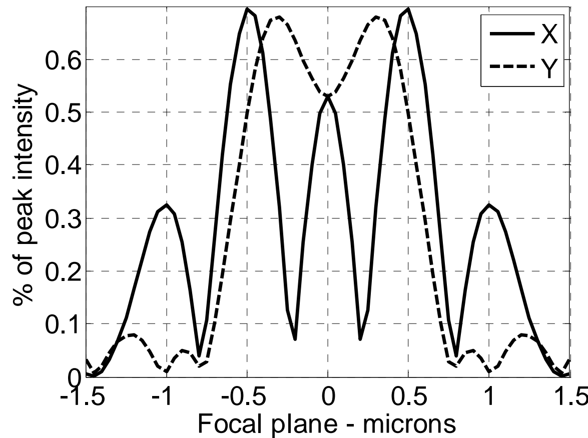

Fig. 7. Absolute difference (in percents of peak intensity) of $|E|^2$ between electric field calculated using paraxial, scalar operators and electric field obtained from rigorous calculations using the Richards-Wolf approach. The ellipticity, corresponding to the simulated NA=0.4, of the rigorously calculated field is represented by the two orthogonal cross sections along x and y.

4.2 Thin optical element approximation

When considering optical elements with a distinguished direction, the way of their interaction with light may depend on polarization. Moreover, when these elements feature nanoscale dimensions, a rigorous, vector simulation of their interaction with light may be due. We examine these issues next.

So far we have dealt with wavefronts and object with one-dimensional variation normal to the propagation direction. The other dimension, normal to both the propagation dimension and to the characteristic dimension, is considered to be infinite, such that the problem does not vary along that dimension. Although for the scalar model it made no difference, in the vector model we consider two cases: the first when the electric field is directed along the infinite dimension and the second when the magnetic field is directed along the infinite dimension referred to as TE and TM components, respectively. The corresponding rigorous vector simulations were performed using COMSOL MULTIPHYSICS™

software, based on Finite Element Method (FEM) analysis. The recording plane intensity distributions in this case were calculated using the Stratton-Chu formula for the far field.

An electric field was calculated at the recording plane by both scalar, paraxial operator method and by FEM. As mentioned above, FEM analysis produced electric fields for the two cases, TE and TM. The results are shown in Fig. 8.

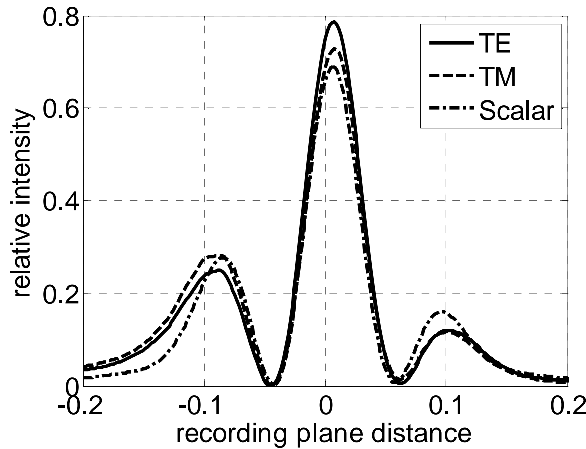

Fig. 8. Electric field intensity at the recording plane. TE, TM correspond to rigorous vector simulations, Scalar corresponds to paraxial, scalar simulation. The phase step is situated in the vicinity of the focal DB center.

The intensity profiles of Fig. 8 exhibit differences both between rigorous and scalar results and between TE and TM themselves. Although the actual values may change as a function of phase step position relative to the DB intensity distribution it is readily observed that the maximum intensity difference between TE and TM is about 5% of peak intensity. This anisotropy has important implications but its treatment is outside the scope of this work..

A more important result is the difference between the normalized intensity distribution corresponding to scalar, paraxial approximation result and the normalized intensity distribution corresponding to rigorous vector results.

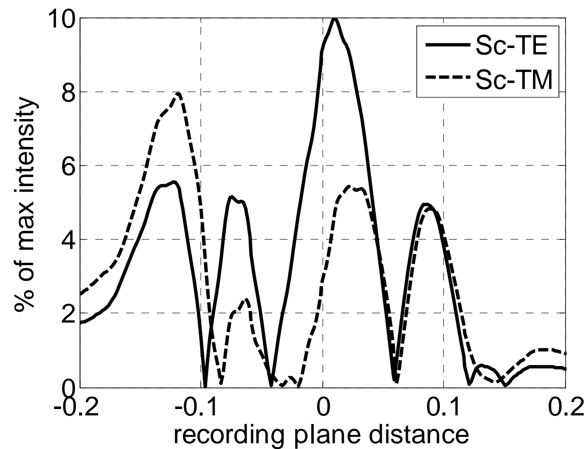

Fig. 9. Absolute value of the difference, in percents of maximum intensity at the recording plane, between normalized result of scalar, vector simulation and normalized results of rigorous, vector simulations, as shown in Fig. 8. Solid line corresponds to the absolute value of the difference between scalar result and TE result while the dashed line corresponds to the TM result.

Fig. 9 presents plots of the absolute values of the differences between the normalized scalar result and the two components of the vector as presented in Fig. 8. The differences are given as percents of the maximum intensity value over the recording plane with the phase step positioned at the DB center. In this case the maximum error due to the scalar approximation is about 10% of the peak intensity and it may reach up to 15% for other relative positions between the

phase step and the DB. Nevertheless, it should be kept in mind that such high error values are present only at certain locations along the recording plane while for the rest of the recording plane the error is below of 5%.

5. ERROR CONSIDERATIONS OF SENSITIVITY

5.1 Sensitivity evaluation

The results presented in the previous section indicate that although the inaccuracies due to numerical aperture are relatively low – about 1%, the errors due to the representation of investigated objects as thin optical elements are somewhat significant – reaching 15%. Fortunately, as long as we can treat optical fields as being continuous (at the relevant scale), this intensity error becomes less important since we calculate the sensitivity as an output intensity difference between two consecutive positions. For example, the sensitivity for a 5 nm position change of the phase step, that corresponds to the output intensities of Fig. 8, is shown in Fig. 10. The vertical axis represents percents of maximum output intensity. Clearly, the errors in sensitivity values do not exceed 0.1% of maximum output intensity.

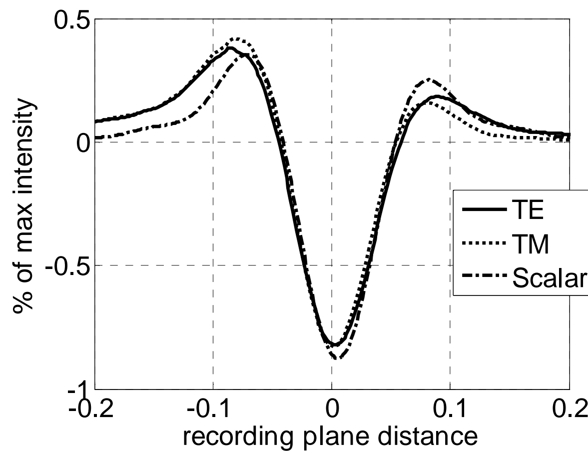

Fig. 10. Change in the output intensity distributions of Fig. 8 for a 5 nm shift in the position of the phase step.

An example for experimental sensitivity analysis is shown Fig. 11. The sensitivity to a position shift of the phase step is calculated as a relative difference between total window powers corresponding to consecutive phase step positions. The sensitivity is plotted against phase step position relative to the DB. In fact, the curves in Fig. 11 are derivatives of the corresponding curves in Fig. 6.

In this case, the difference between scalar simulation and experiments is of the same order as the difference between different experiments. This is probably due to various distortions that were present in the experimental setup and the fact that the window power analysis method averages intensity over a certain area, thus mitigating the influence of local errors.

It is noteworthy that an experimental prototype DB microscopic system exhibits sensitivity of about 20nm.

5.2 Sensitivity capabilities of DB microscopy

The experimental results described above correspond to a specific laboratory system and they do not represent the full potential of DB microscopy. For instance, the focal intensity distribution for an ideal case (of NA=0.4), as shown in Fig. 2, is about three times thinner than the corresponding focal intensity distribution of the experimental singular beam. Therefore additional paraxial, scalar simulations were performed to investigate the capabilities of DB microscopy.

The additional capability simulations assumed an ideal optical system with NA=0.4 and SNR=30dB. Similar to the above, these simulations used a phase step as an object model. The simulations checked two cases: phase step shift and phase step height change. As it is demonstrated in Fig. 11, the sensitivity is not uniform across various phase step positions. Similarly it is not uniform across various phase step heights. Consequently, a sensitivity cutoff value was chosen such that it will hold for approximately 80% of phase step situations (positions in the case of phase step lateral movement). This ensures that the following simulation results have practical, rather that purely theoretical meaning. The

results are: 2.5nm sensitivity for lateral phase step shift and 1.25nm sensitivity for phase step height change. In the course of result derivation an assumption was used that the optical field is continuous for the involved scale.

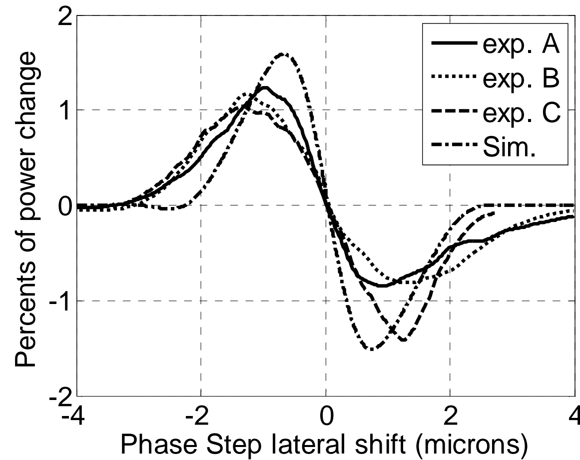

Fig. 11. Total window power sensitivity as a function of phase step position. The results are normalized to 20nm phase step shift that was used in experiment C. Vertical axis is in percents of maximum window power, horizontal axis is phase step shift in microns. Semi dotted curve is simulation, other curves – experiments.

These remarkable results were obtained for surface objects possessing some nanoscale features, which can be successfully approximated by thin optical elements (where paraxial, scalar simulation errors relative to rigorous, vector treatment, are kept at the acceptable level). As for surface objects of nanoscale dimensions, where paraxial, scalar treatment produces errors of the same order as the result, a full set of rigorous, vector simulations must be carried out so as to obtain a credible result.

6. CONCLUSIONS

A modeling procedure for SB microscopy was presented with the help of a case study involving a DB microscope and a phase step as an object. For the analysis of the measurement data emphasis was placed on the possibility of real-time on-line processing. The high speed of analysis, enabled by paraxial, scalar simulation approach had its price though, when accuracy was concerned. A comparison of simulation results with a rigorous vector model yielded partial errors as high as 15% (of peak intensity), while a typical error was of an order of 5%. In spite of that, the corresponding sensitivity, due to its differential nature, exhibited similarity both between scalar simulations and rigorous simulations and between scalar simulations and experiments. DB microscopy sensitivity capabilities, as predicted by paraxial, scalar simulations, were found to be of the order of 1nm.

Acknowledgements

This work was performed within the NANOPRIM project supported by the European Community under the FP6 program. B. Spektor was also partially supported by the Center for Absorption in Science, Ministry of Immigrant Absorption, State of Israel.

REFERENCES

1. B. Spektor, G. Toker, J. Shamir, M. Friedman, A. Brunfeld, "High resolution surface feature evaluation using multi-wavelength optical transforms", in Proc. SPIE **4777,** *Interferometry XI: Techniques and Analysis*, 345-351 (2002).
2. G. Toker, A. Brunfeld, J. Shamir, B. Spektor, E. Cromwell, J. Adam, "In-line optical surface roughness determination by laser scanning", in Proc. SPIE **4777,** *Interferometry XI: Techniques and Analysis*, 323-329 (2002).

3. A. Tavrov, N. Kerwien, R. Berger, H. Tiziani, M. Totzek, B. Spektor, J. Shamir, G. Toker and A. Brunfeld, "Vector simulations of dark beam interaction with nano-scale surface features", *in Optical Measurement Systems for Industrial Inspection III*, SPIE Proc. 5144, 26-36 (2003).
4. B. Spektor, A. Normatov and J. Shamir, "Experimental validation of 20nm sensitivity of Singular Beam Microscopy" to be published in Proc. SPIE **6617,** *Optical Measurement Systems for Industrial Inspection V*, Munich, June 2007.
5. J. Shamir, *Optical Systems and Processes*, SPIE, 1999.
6. M. S. Soskin (ed.) Singular optics, Proc. SPIE, **3487** (1998).
7. J. F. Nye and M. V. Berry, "Dislocations in Wave Trains", *Proc. R. Soc. Lond. A.* **336**, 165-190 (1974).
8. J.V. Hajnal, "Singularities in the transverse fields of electromagnetic waves. I. Theory", Proc. R. Soc. Lond. A 414, 433-446 (1987); "Singularities in the transverse fields of electromagnetic waves. II. Observations of the electric field", ibid 447-468 (1987).
9. G. Indebetouw, "Optical vortices and their propagation", Journal of Modern Optics, **40**, 73-87 (1993).
10. I.V. Basistiy, MS. Soskin, M.V. Vasnetsov, "Optical wavefront dislocations and their properties", Opt. Comm. **119**, 604-612 (1995).
11. M.S. Soskin, V.N. Gorshkov, M.V.Vasnetsov, J.T.Malos, N.R.Heckenberg, “Topological charge and angular momentum of light beams carrying optical vortices”, Phys.Rev. A, **56**, 4064-4075 (1997).
12. I. Dana, I. Freund, "Vortex-lattice wave fields", Opt. Comm. **136**, 93-113 (1997).
13. I. Freund, "Vortex derivatives", Opt. Comm. **137**, 118-126 (1997).
14. Y. J. Schechner and J. Shamir, “Parametrization and orbital angular momentum of anisotropic dislocations”, J. Opt. Soc. Am. A **13**, 967-973 (1996),
15. L. Allen, M. J. Padgett and M. Babiker, “The orbital angular momentum of light”, Progress in Optics, **39,** 294-372 (1999).
16. W.M. Lee, X.-C. Yuan, K. Dholakia, "Experimental observation of optical vortex evolution in a Gaussian beam with an embedded fractional phase step", Opt. Comm. **239**, 129–135 (2004).
17. M. S. Soskin, V. Denisenko and I. Freund, "Optical polarization singularities and elliptical stationary points" Opt. Lett. **28**(16), 1475-1477, (2003).
18. B. Spektor R. Piestun, and J. Shamir, "Dark Beams with a constant notch", Opt. Letters **21**, 456-458 (1996).
19. Y. Parkhomenko, B. Spektor and J. Shamir, "Laser mode selection by combining a bi-prism-like reflectors with a narrow amplitude masks" Appl. Opt. **45**(12), 2761-2765, (2006).
20. B. Richards and E. Wolf, “Electromagnetic diffraction in optical systems, II Structure of the image field in an optical system”, *Proc. R. Soc. Lond. A.* **253**, 358-379 (1959).